Mechatronics 77 (2021) 102583

Contents lists available at ScienceDirect

Mechatronics

journal homepage: www.elsevier.com/locate/mechatronics

An adaptive hierarchical control approach of vehicle handling stability improvement based on Steer-by-Wire Systems ☆

Haohan Yang [a], Wentong Liu [b,c], Li Chen [b], Fan Yu [a,*]

[a] School of Mechanical Engineering, Shanghai Jiao Tong University, Shanghai, China
[b] School of Naval Architecture, Ocean & Civil Engineering, Shanghai Jiao Tong University, Shanghai, China
[c] National Engineering Laboratory for Marine and Ocean Engineering Power System, Shanghai, China

ARTICLE INFO

Keywords:
Steer-by-Wire (SbW) system
Variable steering ratio (VSR) strategy
Active front steering (AFS)
Sliding mode control

ABSTRACT

This paper proposes a novel adaptive hierarchical control approach for Steer-by-Wire (SbW) vehicles to improve the handling stability. The high-level stability control scheme contains a variable steering ratio (VSR) strategy based on the adaptive-network-based fuzzy inference system (ANFIS) and an active front steering (AFS) controller designed with the integral sliding mode method by tracking the expected yaw rate, in which the desired front wheel angle is generated to enhance the cornering stability performance. Besides, an adaptive tracking controller (ATC) for the SbW system is designed by using the adaptive sliding mode control method to achieve desired steering performance in the lower level. The proposed adaptive control strategy is validated with different driving circles from ISO standards in simulation tests and hardware-in-the-loop (HiL) experiments. The results demonstrate that the designed control approach improve the vehicle handling stability significantly, even in some extreme driving conditions.

1. Introduction

In recent years, road vehicle automation has become an increasingly popular research topic in both academia and industry. Advanced driver assistance system (ADAS) plays an important role in vehicle intelligence developments, while Steer-by-Wire (SbW) system of the automobile is recognized as an important one for ADAS [1]. Due to its high efficiency and flexibility in communication and control integration, SbW systems provide a necessary hardware condition for the vehicle autonomous steering.

As the primary aspect of vehicle dynamics and safety, vehicle handling performance is greatly influenced by the steering system. In [2], Shimizu et al. found that the larger steering wheel angle would generate increased driver's physical workload at low speeds, conversely, the meticulous steering operation with a relatively small angle would increase the mental workload at high speeds. Some variable gear ratio steering methods based on specific mechanical actuators were developed to improve the vehicle steering stability [3,4], but their accuracy and reliability may not be guaranteed in practice due to the mechanical wear. Since the mechanical linkage between the steering column and the actuator is removed in SbW systems, the steering control with a variable transmission ratio can be realized without hardware limitations. By using a fuzzy adaptation method, Azzalini et al. [5] presented a variable steering ratio (VSR) approach with the temporal gradient to determine the 'danger' level of driving situations. Wu et al. [6] proposed a multi-objective evaluation scheme to further optimize the VSR strategy according to vehicle motion states, but the steering ratio only can be achieved as discrete values.

Active steering control plays an extremely important role in active safety systems, which is devoted to improving the vehicle cornering stability by providing an additional steering angle. In the previous researches, many efforts have been spent on various control approaches. Falcone et al. [7] proposed a predictive control model based on the online linearization of a vehicle model to reduce the computational complexity. The controller with a disturbance observer based on the SbW system was designed to guarantee the robust yaw stability by Nam et al. [8]. It is also quite common for researchers to integrate the steering system with other active systems to achieve better handling performance [9–12]. These studies all emphasized the coordination among different sub-systems, but these proposed methods were only examined by simulations. In contrast, sliding mode control techniques have been widely applied in engineering practice since it does not require an accurate mathematical model. Some different sliding mode structures were designed to improve the vehicle cornering stability with strong robustness [13–15], in which the driver's input is adopted

☆ This paper was recommended for publication by Associate Editor Yan Chen.

* Corresponding author.
E-mail address: fanyu@sjtu.edu.cn (F. Yu).

https://doi.org/10.1016/j.mechatronics.2021.102583
Received 30 August 2020; Received in revised form 30 December 2020; Accepted 23 May 2021
Available online 30 June 2021

as the reference to calculate the desired yaw rate. Therefore, vehicle manipulation characteristics would be fuzzy due to discontinuous front angle compensations, especially under critical driving conditions.

In order to enable SbW systems to possess similar characteristics as conventional steering systems, many control strategies have been developed for the steering actuator to track desired steering inputs accurately. A linear proportional-derivative (PD) controller was presented for tracking the desired front wheel angle in [16], but the inherent large overshoot generated by its integral term cannot be avoided. In [17,18], a steering control model combined with an online adaptive parameter estimator was proposed. However, these methods cannot eliminate the effects of disturbances in real driving conditions. Wang et al. [19,20] utilized a sliding mode controller with good robustness to reduce the influence of parameter perturbations, but its tracking performance would degenerate significantly with large disturbances. Zhu et al. [21] developed a composite internal model control approach to deal with external disturbances, but its tracking precision would be poor when the nominal model mismatched the SbW system. Some intelligent tracking controllers were proposed to achieve better performance [22–24]. For instance, a radial basis function neural network was adopted to adaptively learn the uncertainty bound [23], which can effectively reduce the influence of parametric uncertainties in steering systems. Nevertheless, these proposed methods were rarely applied in engineering applications due to their high computational complexities.

In this paper, an adaptive hierarchical control approach is proposed to improve the cornering stability and tracking performance of the SbW system. The main contributions are summarized as follows:

(I) A learning-based VSR strategy is proposed to optimize the steering ratio quantitatively by introducing a compensating coefficient, in which the steering ratio is adjusted according to the vehicle states in real time.

(II) An active steering controller using the integral sliding mode technique is designed to acquire the desired front angle based on time-varying vehicle states, which can be robust against the existing vehicle parametric uncertainties.

(III) An adaptive tracking controller (ATC) is designed for the SbW system to realize the desired front wheel angle obtained from the upper level, in which an adaptive law using for online estimation of the switching gain is introduced to avoid the uncertainty bound of disturbances.

The rest of this paper is organized as follows. In Section 2, the mathematical model for the reference vehicle model and the SbW actuator are established, respectively. In Section 3, a novel hierarchical control framework consisting of an active steering scheme with a learning-based variable gear ratio strategy and an adaptive tracking scheme used for following the steering command automatically is developed. Section 4 analyzes the simulation and experimental results of the proposed control approach in different operation conditions. Conclusions and some further work are given in Section 5.

2. System modeling

2.1. Vehicle model

A 2-DOF linear single-track vehicle model, with two degrees of freedom for yaw and lateral motions, is employed for the active front steering (AFS) controller design, as shown in Fig. 1. Despite the reduced complexity, the 2-DOF vehicle model captures primary handling characteristics and thus is widely used in controller design as the reference model [25]. According to Fig. 1, the lateral and yaw movement in this model can be described as

$$m\left(v_y + v_x\gamma_r\right) = F_f + F_r \tag{1a}$$

$$I_z\dot{\gamma}_r = aF_f + bF_r \tag{1b}$$

where m is the vehicle mass, I_z represents the vehicle yaw moment of inertia, v_x and v_y are the vehicle forward speed and lateral velocity

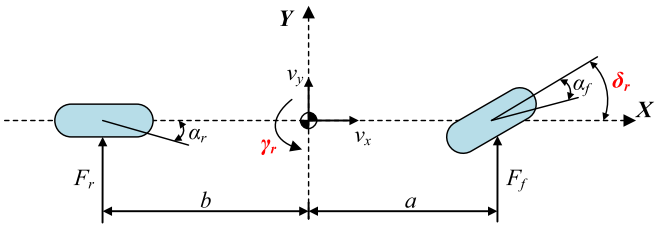

Fig. 1. 2-DOF single track vehicle model.

respectively, a and b are distances from the center of gravity (c.g.) to front and rear axles respectively, F_f and F_r are lateral tyre forces of front and rear wheels, respectively, which can be defined as $F_f = C_f\alpha_f$, $F_r = C_r\alpha_r$ with the assumption of a small tyre sideslip angle, C_f and C_r denote the cornering stiffness of front and rear wheels, respectively, α_f and α_r are front and rear wheel sideslip angles that can be represented respectively as

$$\alpha_f = \delta_r - \frac{v_y + a\gamma_r}{v_x} \tag{2a}$$

$$\alpha_r = \frac{v_y - b\gamma_r}{v_x} \tag{2b}$$

where δ_r is the desired front wheel steering angle that is comprised of driver's input and an additional steering angle introduced by the AFS controller.

Substituting Eq. (1) into Eq. (2), the equation of the vehicle model motion can be rewritten in a state-space format as

$$\begin{bmatrix}\dot{v}_y\\ \dot{\gamma}_r\end{bmatrix} = \begin{bmatrix}-\frac{C_f+C_r}{mv_x} & -\frac{aC_f-bC_r}{mv_x}-v_x\\ -\frac{aC_f-bC_r}{I_zv_x} & -\frac{a^2C_f+b^2C_r}{I_zv_x}\end{bmatrix}\begin{bmatrix}v_y\\ \gamma_r\end{bmatrix} + \begin{bmatrix}\frac{C_f}{m}\\ \frac{aC_f}{I_z}\end{bmatrix}\delta_r \tag{3}$$

2.2. Steering actuator model

The architecture of the steering actuator module is briefly described in Fig. 2. Compared with traditional steering systems, SbW systems remove the mechanical linkage between steering columns and steering actuators. According to previous studies of steering dynamics modeling [19,20], the SbW system can be considered as a rigid body. Accordingly, the dynamic model of the steering actuator module is given as below,

$$J_{eq}\ddot{\delta}_a + B_{eq}\dot{\delta}_a + \tau_e + \tau_f = i_{cr}\cdot\tau_m \tag{4a}$$

$$J_{eq} = J_{fw} + i_{cr}^2J_m \tag{4b}$$

$$B_{eq} = B_{fw} + i_{cr}^2B_m \tag{4c}$$

where J_{eq} and B_{eq} are the equivalent inertia and damping of the SbW system respectively, τ_e is the tyre self-aligning torque, τ_f is the system friction torque, i_{cr} denotes the combined steering ratio including the planetary gear reducer and the rack & pinion gearbox, τ_m is the output torque of the steering actuating motor, and δ_a, $\dot{\delta}_a$, $\ddot{\delta}_a$ represent the angular position, angular velocity and angular acceleration of the front wheel, respectively. Besides, J_{fw} and J_m are moments of inertia of front wheels and the steering motor respectively, while B_{fw} and B_m are damping coefficients of front wheels and the steering motor, respectively.

3. Adaptive hierarchical controller design

The task of handling stability control of SbW vehicles is to track the expected yaw rate and the desired front wheel angle accurately. Considering the parametric uncertainties, unpredictable external disturbances and particular transmission features of SbW systems, a novel

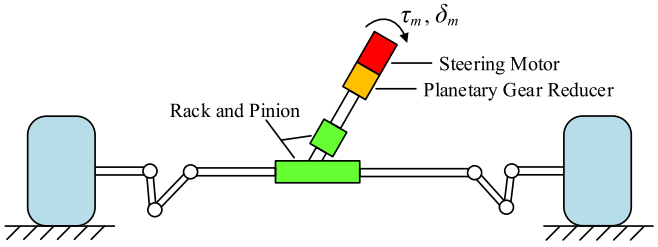

Fig. 2. Architecture of steering actuator.

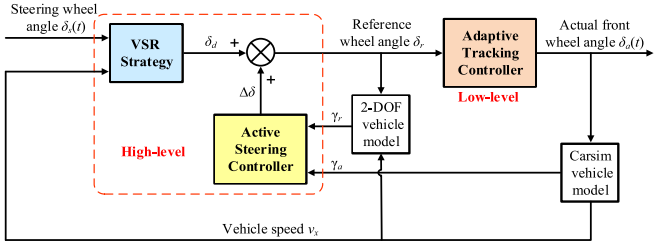

Fig. 3. Schematic diagram of the designed adaptive hierarchical control approach.

active hierarchical control strategy containing two levels is designed in this section. The corresponding schematic diagram of the proposed control scheme is described in Fig. 3.

3.1. Variable steering ratio design

To improve the steering agility, a relatively small steering ratio is desired at low driving speeds. In comparison, an increased transmission ratio is required to enhance steering stability and safety at high speeds. Based on the SbW system, a learning-based VSR strategy is developed to achieve an ideal variable steering ratio.

Suppose that the steering wheel angle is δ_s and the front wheel angle from the driver's input is δ_d. Therefore, the steering ratio of the SbW system is described as

$$i_{ds} = \frac{\delta_s}{\delta_d} = \beta i_{cr} \tag{5}$$

where β represents the compensating coefficient generated by the designed VSR strategy.

The yaw rate gain is a critical parameter to reflect the vehicle handling performance during the steering control. With the definition of the yaw rate generated by the driver's input as γ_d, the vehicle yaw rate gain can be obtained as

$$G_s^\gamma = \frac{\gamma_d}{\delta_s} \tag{6}$$

Based on the ISO standard [26], step steering numerical tests are conducted with specified vehicle speeds. Fig. 4 demonstrates the characteristics of the yaw rate gain with a fixed steering ratio. It can be seen that the yaw rate gain G_s^γ reduces nonlinearly with the increased steering wheel angle, which makes the steering manipulation hard especially in drastic driving conditions with extensive steering angles. Therefore, in this study, the transmission ratio compensation is developed to achieve an invariable yaw rate gain with respect to different steering wheel angles. Also, it can be observed in Fig. 4 that a relatively invariable gain appears in the certain steering wheel angle range, which is selected as the desired yaw rate gain for the specific vehicle speed. Based on the Eq. (5), the transmission ratio compensating coefficient is calculated as

$$\beta = \frac{\delta_s}{i_{cr}\delta_d} = \frac{\delta_s G_d^\gamma}{i_{cr}\gamma_d} = \frac{G_d^\gamma}{i_{cr}G_s^\gamma} \tag{7}$$

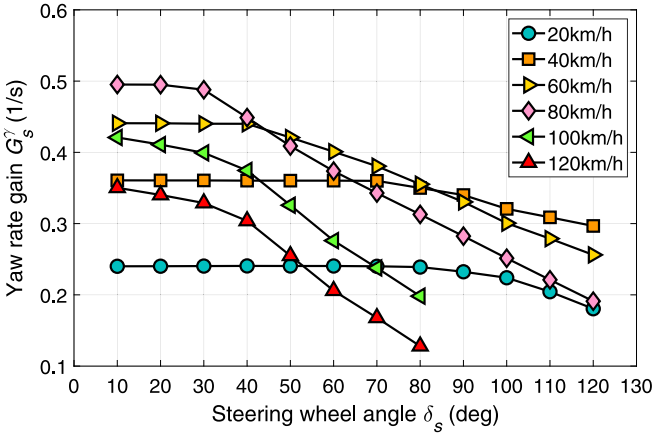

Fig. 4. Yaw rate gain characteristics versus different steering wheel angles for specific vehicle speeds with a fixed steering ratio.

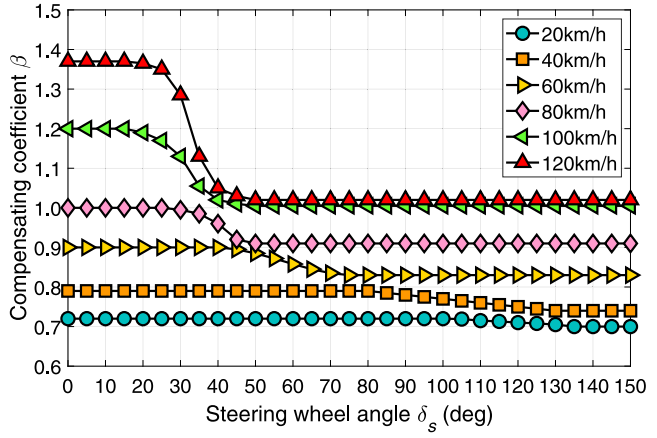

Fig. 5. Variable steering ratio characteristics versus different steering wheel angles for specific vehicle speeds.

Table 1
Key parameters of proposed ANFIS.

Parameter	Value
Training epochs	1000
Learning rate	0.3
Gradient	1.0e−7
Weights initialization	random
Validation error	1.0e−4

where G_d^γ denotes the gain from the yaw rate to the front wheel angle that is derived from Eq. (3) as

$$G_d^\gamma = \frac{\gamma_d}{\delta_d} = \frac{v_x/(a+b)}{1 + \frac{m}{(a+b)^2}\left(\frac{b}{C_f} - \frac{a}{C_r}\right)v_x^2} \tag{8}$$

Fig. 5 shows the optimized steering ratio characteristics with different steering angles in specified vehicle forward speeds. The relatively linear vehicle yaw rate based on the compensation of steering ratio would improve the handling performance of the SbW vehicle [6]. Essentially, it can be regarded as a complicated nonlinear multiple-input single-output (MISO) system. The adaptive-network-based fuzzy inference system (ANFIS) was proposed by Jang [27] firstly, which has been widely adopted in advanced control systems. In this study, an ANFIS is designed to optimize the steering ratio in general driving situations. The architecture of the proposed ANFIS with five layers is illustrated in Fig. 6 and introduced in details as follows,

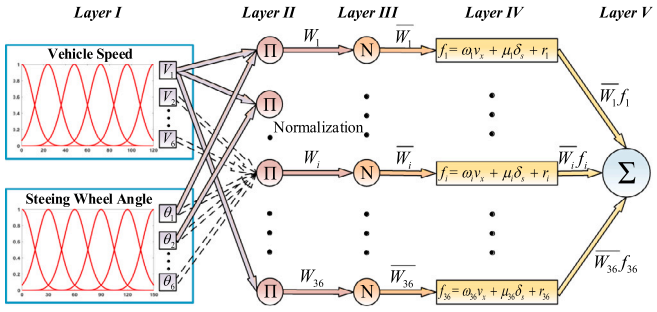

Fig. 6. Architecture of proposed ANFIS.

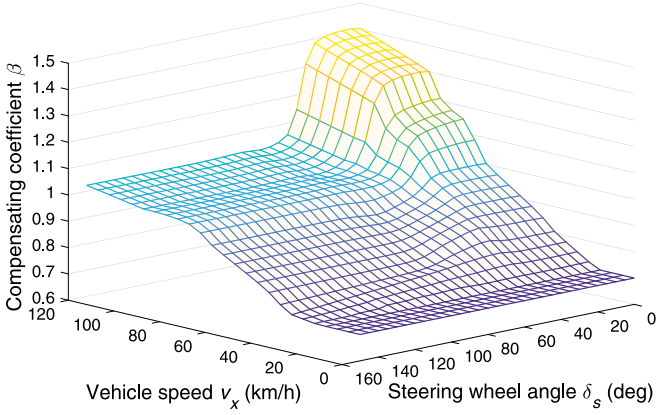

Fig. 7. Fuzzy inference system output surface.

Layer I: *Fuzzified Layer*

The vehicle forward speed v_x and the steering wheel angle δ_s are input variables. Every node in the fuzzified layer is assigned a Gaussian member function with modifiable parameters as below,

$$O_k^1 = \begin{cases} \mu_m^V(v_x) = \exp\left\{-\dfrac{(x-d_m)^2}{2\sigma_m^2}\right\} \\ \mu_n^\theta(\delta_s) = \exp\left\{-\dfrac{(x-d_n)^2}{2\sigma_n^2}\right\} \end{cases} \tag{9}$$

where m, n=1~6, k=max(m+ n) is the number of nodes in the first layer, $\{d_m, \sigma_m, d_n, \sigma_n\}$ is referred to as *premise parameters* set.

Layer II: *Participation layer*

Each node in the participation layer computes the multiplication of the incoming signals, and therefore, the output of ith node in layer II is generated as

$$O_i^2 = \mu_m^V(v_x) \cdot \mu_n^\theta(\delta_s) = W_i \tag{10}$$

where W_i is called the firing strength of the ith node. Each node corresponds to an "if-then" rule of Takagi and Sugeno's (T-S) type.

Layer III: *Normalization layer*

The ith node in the normalization layer calculates the ratio of the firing strength to the sum of all rules' firing strengths,

$$O_i^3 = \frac{W_i}{W_1 + W_1 + \cdots + W_s} = \frac{W_i}{\sum_{i=1}^{s} W_i} = \overline{W}_i \tag{11}$$

Layer IV: *Defuzzification layer*

Each node in the defuzzification layer is a multiplication of the normalized firing strength and the corresponding first-order polynomial f_i assumed as $\omega_i v_x + \mu_i \delta_s + r_i$. Consequently, the output of ith node in this layer is given by

$$O_i^4 = \overline{W}_i f_i = \overline{W}_i(\omega_i v_x + \mu_i \delta_s + r_i) \tag{12}$$

where $\{\omega_i, \mu_i, r_i\}$ is referred to as *consequent parameters* set.

Layer V: *Output layer*

In the output layer, compensating coefficient β is generated as

$$O_1^5 = \sum_{i=1}^{s} O_i^4 = \sum_{i=1}^{s} \overline{W}_i f_i = \beta \tag{13}$$

In the architecture of ANFIS, precise parameters and consequent parameters are optimized using a composite algorithm combined by the least squares estimator (LSE) and the Levenberg–Marquardt (LM) method. Normally, system parameters of a specific vehicle will not change significantly in a short period, so we adopt the batch learning to avoid the high computational complexity during driving. Simulation results of the VSR shown in Fig. 5 are selected as the training dataset. Key parameters and the output surface of ANFIS are shown in Table 1 and Fig. 7, respectively.

3.2. Active steering controller design

To improve the stability of manipulating steering operation, especially in some critical driving situations, the AFS controller is designed by using an integral sliding mode control (ISMC) method.

According to the 2-DOF vehicle model shown in Fig. 1, the expected yaw rate can be derived under the steady-state cornering condition as below,

$$\gamma_r = \frac{v_x/(a+b)}{1 + \dfrac{m}{(a+b)^2}\left(\dfrac{b}{C_f} - \dfrac{a}{C_r}\right)v_x^2}\delta_r \tag{14}$$

Therefore, the tracking error can be defined as

$$e_\gamma = \gamma_a - \gamma_r \tag{15}$$

Then the sliding variable is defined, and its derivative can be obtained as

$$s_\gamma = e_\gamma + \Lambda \int e_\gamma dt \tag{16a}$$

$$\dot{s}_\gamma = \dot{e}_\gamma + \Lambda e_\gamma \tag{16b}$$

where Λ is a designed positive constant.

Substituting Eq. (15) into Eq. (16b), the following equation can be obtained

$$\begin{aligned} \dot{s}_\gamma &= \dot{e}_\gamma + \Lambda e_\gamma = \dot{\gamma}_a - p_1 v_y - p_2 \gamma_r - p_3 \delta_r + \Lambda e_\gamma \\ &= p_3\left(\frac{1}{p_3}(\dot{\gamma}_a + \Lambda e_\gamma) - \frac{p_1}{p_3}v_y - \frac{p_2}{p_3}\gamma_r - \delta_r\right) \\ &= p_3\left(\left[\frac{1}{p_3} - \frac{p_1}{p_3} - \frac{p_2}{p_3}\right]\begin{bmatrix} \dot{\gamma}_a + \Lambda e_\gamma \\ v_y \\ \gamma_r \end{bmatrix} - \delta_r\right) \\ &= p_3\left(W^T\phi - \delta_r\right) \end{aligned} \tag{17}$$

where $p_1 = -\dfrac{aC_f - bC_r}{I_z v_x}$, $p_2 = -\dfrac{a^2C_f + b^2C_r}{I_z v_x}$, $p_3 = \dfrac{aC_f}{I_z}$.

It can be observed from Eq. (17) that the idealized control input is $\delta_r = W^T\phi$. Due to the existing parametric uncertainties, a changeable vehicle yaw moment of inertia range can be assumed within the $[I_{z\min}, I_{z\max}]$, thus the nominal value is defined as

$$\hat{I}_z = \sqrt{I_{z\min} \cdot I_{z\max}} \tag{18a}$$

Similarly, the nominal values of tyres cornering stiffness can be defined as

$$\hat{C}_f = \sqrt{C_{f\min} \cdot C_{f\max}} \tag{18b}$$

$$\hat{C}_r = \sqrt{C_{r\min} \cdot C_{r\max}} \tag{18c}$$

Therefore, the corresponding nominal values of $\hat{p}_1$, $\hat{p}_2$, $\hat{p}_3$ can be achieved. Meanwhile, these parameters need to satisfy the bounded conditions as below,

$$\left|p_1 - \hat{p}_1\right| < \Delta p_1 \tag{19a}$$

$$\left|p_2 - \hat{p}_2\right| < \Delta p_2 \tag{19b}$$

$$\left|p_3 - \hat{p}_3\right| < \Delta p_3 \tag{19c}$$

Considering the parameter perturbation exists in the dynamic system, the desired steering angle is designed as

$$\delta_r = \hat{W}^T \phi + k_s s_\gamma \tag{20}$$

where $\hat{W}^T = \left[1, -\hat{p}_1, -\hat{p}_2\right]/\hat{p}_3$, and k_s is the gain of the sliding mode term. The steering angle compensation by AFS controller can be obtained as

$$\Delta\delta = \delta_r - \delta_d \tag{21}$$

Proof. Choosing the Lyapunov function as

$$V_{AFS} = \frac{1}{2} s_\gamma^2 \tag{22}$$

then its derivative is achieved as

$$\begin{aligned} \dot{V}_{AFS} &= s_\gamma \dot{s}_\gamma = p_3 s_\gamma \left[(W - \hat{W})^T \phi - k_s s_\gamma\right] \\ &= p_3 \left[-k_s s_\gamma^2 + s_\gamma \tilde{W}^T \phi\right] \end{aligned} \tag{23a}$$

where $\tilde{W}^T$ is the estimation error matrix.

All the parameters are bounded according to the previous analysis and therefore $\tilde{W}^T\phi$ is bounded. Assuming that $\tilde{W}^T\phi \le \Delta_W$, then

$$\begin{aligned} \dot{V}_{AFS} &\le p_3 \left[-k_s s_\gamma^2 + \frac{1}{2}\left(s_\gamma^2 + \Delta_W^2\right)\right] \\ &= -p_3 \left[\left(2k_s - 1\right) V_{AFS}\right] + \frac{1}{2}\Delta_W^2 \end{aligned} \tag{23b}$$

The solution to the inequality (23b) can be given as

$$\begin{aligned} V_{AFS} \le & e^{-p_3(2k_s-1)(t-t_0)} V_{AFS}\left(t_0\right) \\ & + \frac{p_3 \Delta_W^2}{2} \int_t^{t_0} e^{-p_3(2k_s-1)(t-t_0)} d\tau \\ = & e^{-p_3(2k_s-1)(t-t_0)} V_{AFS}\left(t_0\right) \\ & + \frac{\Delta_W^2}{4k_s - 2}\left(1 - e^{-p_3(2k_s-1)(t-t_0)}\right) \end{aligned} \tag{24}$$

With the selection of $k_s > 1/2$, it can be seen from inequality (24) that

$$\lim_{t\to\infty} V_{AFS}(t) \le \frac{\Delta_W^2}{4k_s - 2} \tag{25}$$

It is concluded that $V_{AFS}(t)$ would converge to $\frac{\Delta_W^2}{4k_s-2}$ in finite time. Therefore, $\dot{V}_{AFS} \le 0$ is always satisfied with an appropriate chosen of feedback gain k_s [28].

Remark 1. In order to smooth the steering angle compensation $\Delta\delta$, a low-pass filter is employed as below,

$$\Delta\delta = \frac{1}{T_f s + 1}\left(\hat{W}^T \phi + k_s s_\gamma\right) - \delta_d \tag{26}$$

where T_f is a filtering time constant, s represents the Laplace operator.

3.3. Adaptive tracking controller design

In order to achieve the excellent steering performance, an adaptive tracking controller (ATC) is designed by using the robust adaptive sliding mode control (RASMC) method. For the convenience of further analyses, in this study, the system friction torque τ_f and the tyre self-aligning torque τ_e are considered as a lump disturbance $d(t)$. Therefore, the system dynamic equations in Eq. (4) is simplified as

$$\ddot{\delta}_a = -q_1 \dot{\delta}_a + q_2 \tau_m - q_3 d \tag{27}$$

where $q_1 = B_{eq}/J_{eq}$, $q_2 = i_{cr}/J_{eq}$, $q_3 = 1/J_{eq}$.

Define the tracking error of the close-loop SbW system as $e_\delta = \delta_a - \delta_r$, so that its second derivative can be given in Eq. (28)

$$\ddot{e}_\delta = \ddot{\delta}_a - \ddot{\delta}_r = -q_1 \dot{\delta}_a + q_2 \tau_m - q_3 d - \ddot{\delta}_r \tag{28}$$

and the sliding mode variable is defined as

$$s_\delta = \dot{e}_\delta - \Gamma e_\delta \tag{29}$$

where $\Gamma > 0$ is a parameter to be designed.

Based on the SbW system in Eq. (27), the output tracking error e_δ would converge to zero in finite time, provided that the control input τ_m is designed as

$$\begin{aligned} \tau_m &= \frac{1}{i_{cr}}\left(B_{eq}\dot{\delta}_a + \Gamma J_{eq}\dot{e}_\delta - \hat{\eta}\,\mathrm{sign}\left(s_\delta\right) - \kappa_1 s_\delta\right) \\ &= \left[q_1 \dot{\delta}_a + \Gamma \dot{e}_\delta - q_3\left(\hat{\eta}\,\mathrm{sign}\left(s_\delta\right) + \kappa_1 s_\delta\right)\right]/q_2 \end{aligned} \tag{30}$$

where η and $\hat{\eta}$ are the switching gain and its estimated value respectively, which are updated by the adaptive law as

$$\dot{\hat{\eta}} = \kappa_2 \left|s_\delta\right| \tag{31}$$

where κ_1 and κ_2 are positive constants.

Proof. Define the Lyapunov function as

$$V_{ATC} = \frac{1}{2} s_\delta^2 + \frac{1}{2} q_3 \kappa_2^{-1} \tilde{\eta}^2 \tag{32}$$

where $\tilde{\eta} = \hat{\eta} - \eta$ denotes the switching gain error, and the time derivative of V_{ATC} is given by

$$\begin{aligned} \dot{V}_{ATC} &= s_\delta \dot{s}_\delta + q_3 \kappa_2^{-1} \tilde{\eta}\dot{\tilde{\eta}} \\ &= s_\delta\left(\ddot{e}_\delta - \Gamma \dot{e}_\delta\right) + q_3 \kappa_2^{-1} \tilde{\eta}\dot{\tilde{\eta}} \\ &= s_\delta\left(-q_1 \dot{\delta}_a + q_2 \tau_m - q_3 d - \ddot{\delta}_r - \Gamma \dot{e}_\delta\right) + q_3 \kappa_2^{-1} \tilde{\eta}\dot{\tilde{\eta}} \end{aligned} \tag{33a}$$

Substituting the control input torque Eq. (30) into Eq. (33a), then

$$\begin{aligned} \dot{V}_{ATC} &= s_\delta\left[-q_3 d - \ddot{\delta}_r - q_3\left(\hat{\eta}\,\mathrm{sign}\left(s_\delta\right) + \kappa_1 s_\delta\right)\right] + q_3 \kappa_2^{-1} \tilde{\eta}\dot{\eta} \\ &= -s_\delta\left(q_3 d + \ddot{\delta}_r\right) - q_3 \left|s_\delta\right| \hat{\eta} - q_3 \kappa_1 s_\delta^2 + q_3 \kappa_2^{-1} \tilde{\eta}\dot{\hat{\eta}} \end{aligned} \tag{33b}$$

Next, substituting the adaptive law Eq. (31) into Eq. (33b),

$$\begin{aligned} \dot{V}_{ATC} &= -s_\delta\left(q_3 d + \ddot{\delta}_r\right) - q_3 \left|s_\delta\right| \hat{\eta} - q_3 \kappa_1 s_\delta^2 + q_3(\hat{\eta} - \eta)\left|s_\delta\right| \\ &= -s_\delta\left(q_3 d + \ddot{\delta}_r + q_3 \eta \left|s_\delta\right|\right) - q_3 \kappa_1 s_\delta^2 \\ &= -q_3\left[s_\delta\left(d + \ddot{\delta}_r/q_3\right) + \eta\left|s_\delta\right|\right] - q_3 \kappa_1 s_\delta^2 \\ &\le -q_3 \left|s_\delta\right|\left[\eta - \left(d + \ddot{\delta}_r/q_3\right)\right] - q_3 \kappa_1 s_\delta^2 \end{aligned} \tag{34}$$

Assuming that the boundary of disturbance satisfies $d(t) \le \zeta$, and η is selected as

$$\eta = \zeta + \ddot{\delta}_r/q_3 + \varepsilon \tag{35}$$

where ε is an arbitrary positive constant. Then the Eq. (34) can be simplified as

$$\dot{V}_{ATC} \le -q_3 \left|s_\delta\right| \varepsilon - q_3 \kappa_1 s_\delta^2 < 0 \tag{36}$$

Therefore, inequality (36) demonstrates that the sliding variable s_δ will converge to zero in finite time, i.e., the sliding mode surface $s_\delta = 0$ in Eq. (29), and then the tracking error e_δ will converge to zero in limited time [28].

Remark 2. Since the signum function involved in the control signal in (30) will cause the high-frequency chattering, we introduced the boundary layer to alleviate the control chattering [28]

$$\tau_m = \left[q_1 \dot{\delta}_a + \Gamma \dot{e}_\delta - q_3\left(\hat{\eta} \cdot \mathrm{sat}\left(s_\delta\right) + \kappa_1 s_\delta\right)\right]/q_2 \tag{37}$$

Table 2
Parameters of vehicle model and SbW system.

Symbol	Description	Value	Unit
m	Vehicle mass	1765	kg
a	Distance from c.g. to the front axle	1.42	m
b	Distance from c.g. to the rear axle	1.68	m
I_z	Vehicle moment of inertia	3234	kg m^2
C_f	Cornering stiffness of the front wheel	79 240	N rad^{-1}
C_r	Cornering stiffness of the rear wheel	106 398	N rad^{-1}
J_{eq}	Equivalent inertia	0.14	kg m s^2
B_{eq}	Equivalent damping	0.8	N s
i_{cr}	Combined steering ratio of gearbox	15.28	

Table 3
Parameters of designed controllers.

Parameter	Value
Λ	12
k_s	100
T_f	0.01
Γ	8
$[q_1, q_2, q_3]$	[5.71, 109.14, 7.14]
$[\kappa_1, \kappa_2]$	[3.5, 500]
ξ	0.15

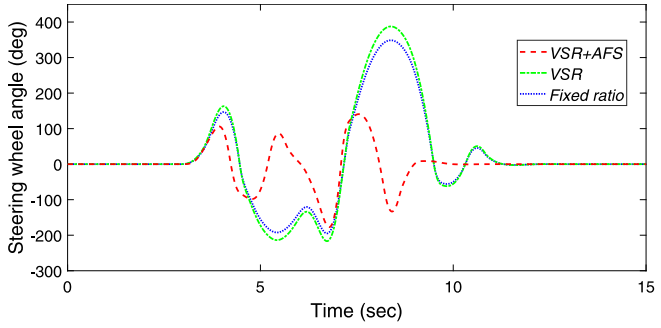

Fig. 8. Steering wheel angle in DLC tests.

where

$$\text{sat}\left(s_\delta\right) = \begin{cases} s_\delta/\xi & |s_\delta| < \xi \\ \text{sign}\left(s_\delta\right) & \text{otherwise} \end{cases} \tag{38}$$

where ξ is a positive constant. It is noted that although the output tracking error e_δ would only converge into the boundary layer rather than zero in limited time, we can still achieve an optimal trade-off between the control bandwidth and the tracking precision by an appropriate choice of ξ in practice.

4. Results and discussions

In order to evaluate the performance of the designed control scheme in Section 3, a series of simulation and experimental tests are conducted in different driving conditions. System parameters of the vehicle model and the SbW plant are presented in Table 2, and the AFS controller and ATC parameters are given in Table 3.

4.1. Simulation experiments

Several simulation tests are conducted based on an established co-simulation platform in the Matlab-Carsim software environment. The high-level stability control scheme is analyzed to examine the improvement of driving stability performance with high robustness. Besides, the steering performance improvement of SbW system is also given to demonstrate the effectiveness of the designed adaptive tracking controller.

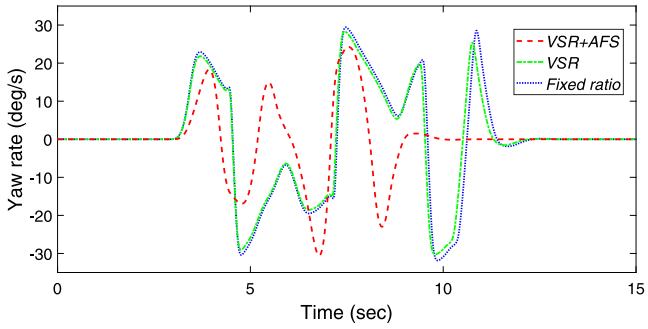

Fig. 9. Yaw rate in DLC tests.

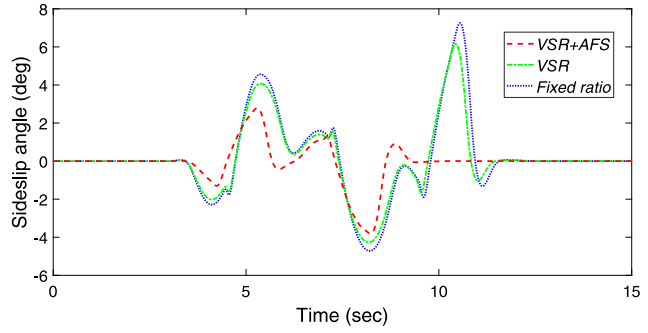

Fig. 10. Sideslip angle in DLC tests.

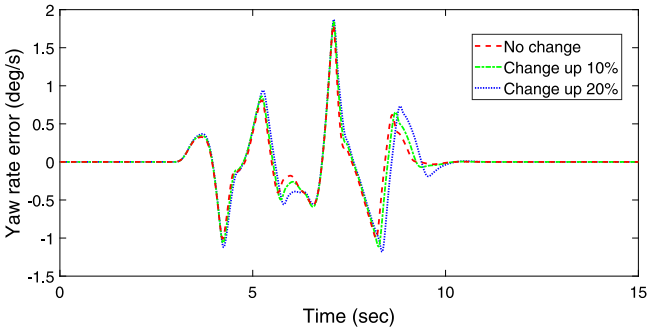

Fig. 11. Yaw rate tracking error in robustness tests.

Based on the ISO standard [29], taking the double-lane change (DLC) test as an example to demonstrate the steering stability improvement of the designed control scheme firstly. The vehicle travels at a high speed of 80 km/h on a slippery road with the road adhesion coefficient set as 0.3. Simulation results including the steering input and vehicle responses are presented in Figs. 8–10. Besides, a traditional fixed transmission ratio scheme as well as the VSR strategy without AFS are adopted to contrast with the presented stability control scheme.

As shown in Fig. 8, it can be seen that a quite large steering wheel angle is required to ensure the trajectory tracking and reach a steady state without the AFS strategy. Vehicle yaw rate and sideslip angle correspondingly present a haphazard and unsteady variation, as shown in Figs. 9 and 10, respectively, which indicates that the vehicle skids between t=5s~10s. By comparison, the proposed stability control scheme presents steadier variations of yaw rate and sideslip angle, demonstrating a significant improvement in stability performance. Besides, it should be noted that the steering wheel angle with VSR is larger than that in the fixed transmission ratio due to the greater transmission ratio of VSR at high vehicle speeds, which helps improve the driving stability with a decrease of the steering sensitivity.

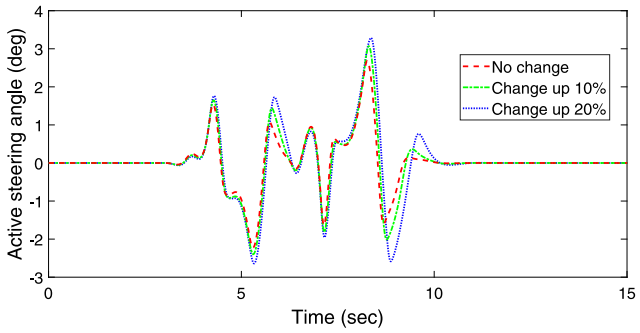

Fig. 12. Compensation of front wheel angle.

Table 4
Parameters of test cycles in simulations.

Maneuver	Velocity	Type	Length
Step steer	80 km/h	4.5 deg Step steering	1 s
Sine sweep	70 km/h	0.2 Hz-1 Hz Sine steering	16 s
Lane change	75 km/h	Standard double-lane change	250 m

Table 5
Characteristic values of test cycles.

Parameter	Weave test	Transition test	Square turn	Serpentine
Max. steering angle (deg)	40	45	600	400
Max. steering velocity (deg/s)	10	5/15/45	400	100
Road adhesion coefficient	0.3	0.4	0.8	0.4
Vehicle forward speed (km/h)	30/60/90	80	60	40

Besides, the robust performance analysis for the designed high-level control scheme is conducted in the same driving conditions as stability tests. The vehicle parameters, i.e., I_z, C_f, C_r, are allowed to vary within 20% of normal values in tests. Figs. 11 and 12 illustrate the response results of yaw rate tracking error and the corresponding front wheel angle compensation introduced by AFS, respectively. It can be seen that the tracking error of yaw rate can converged to zeros under different driving conditions, which demonstrates that the presented stability scheme has good robustness to the vehicular parametric uncertainties and realizes the satisfactory stability performance.

According to ISO standards [26,29], three typical test cycles are adopted as examples to illustrate the tracking performance of the proposed adaptive tracking controller. The details of presented test cycles in simulations are listed in Table 4. Besides, the conventional PD control approach ($\tau_{PD} = -5.8e_\delta - 1.2\dot{e}_\delta$) and the robust sliding mode control method used in [19] with a Kalman disturbance observer (SMC-KL) are employed to compare with the proposed RASMC method. Note that all the control parameters are carefully selected with repeated simulation tests. The tracking performance of the SbW system under different operating conditions are presented in Fig. 13. According to the simulation results, tracking performance of the ATC based on the RASMC method shows better tracking precision than other approaches.

4.2. Experimental verification

Hardware-in-the-loop (HiL) experiments are carried out to further evaluate the performance of the proposed control scheme. As shown in

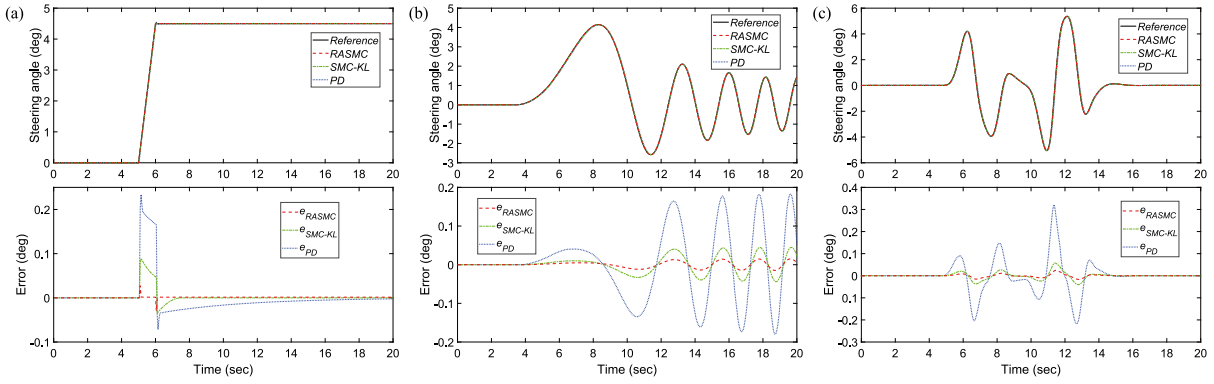

Fig. 13. Comparison of SbW system tracking performance by using different controllers. (a) Step steering. (b) Sweep steering. (c) Lane change.

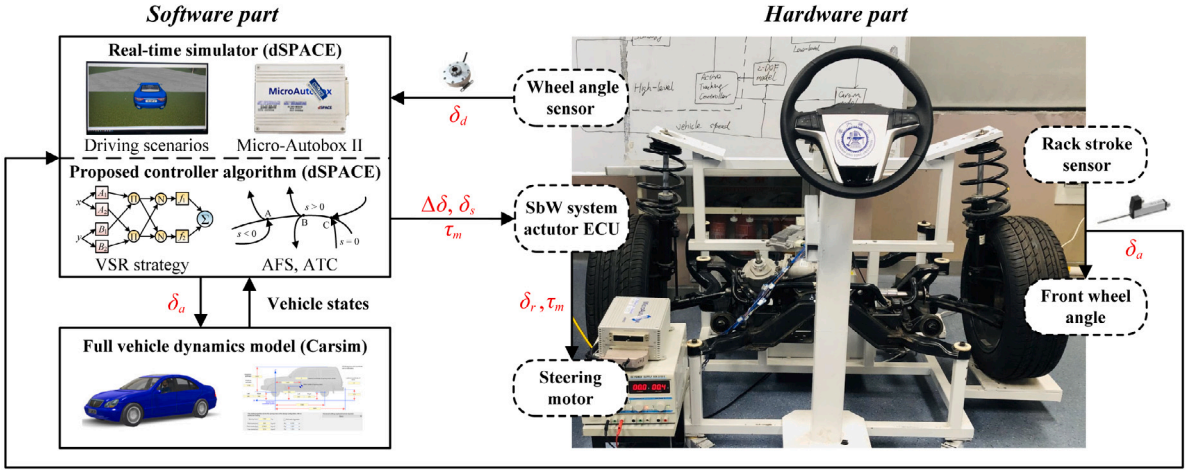

Fig. 14. Schematic diagram of the hardware-in-the-loop experiments.

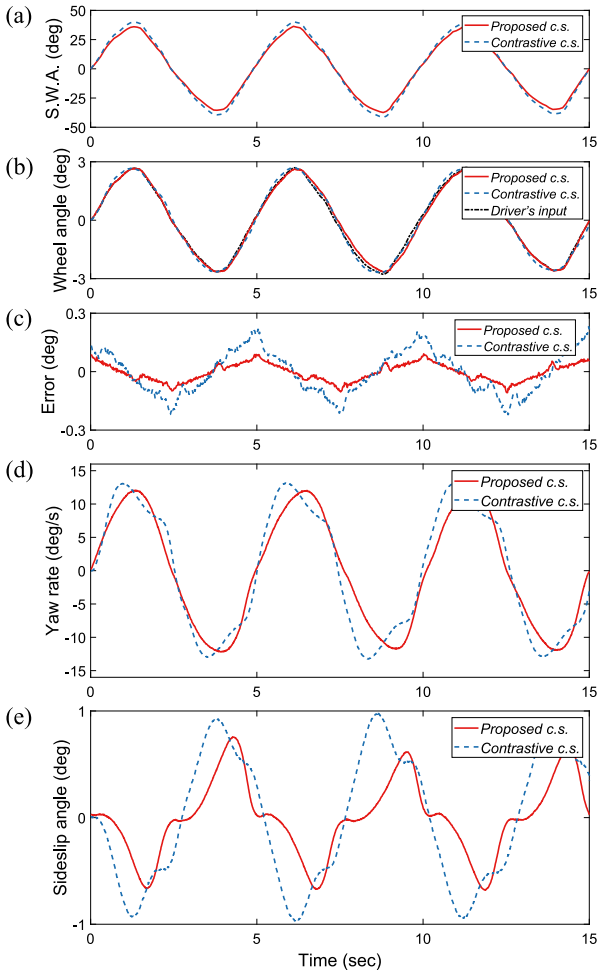

Fig. 15. 40° weave test at vehicle forward speed 60 km/h. (a) Steering wheel angle. (b) Front wheel angle. (c) Tracking error. (d) Yaw rate. (e) Sideslip angle.

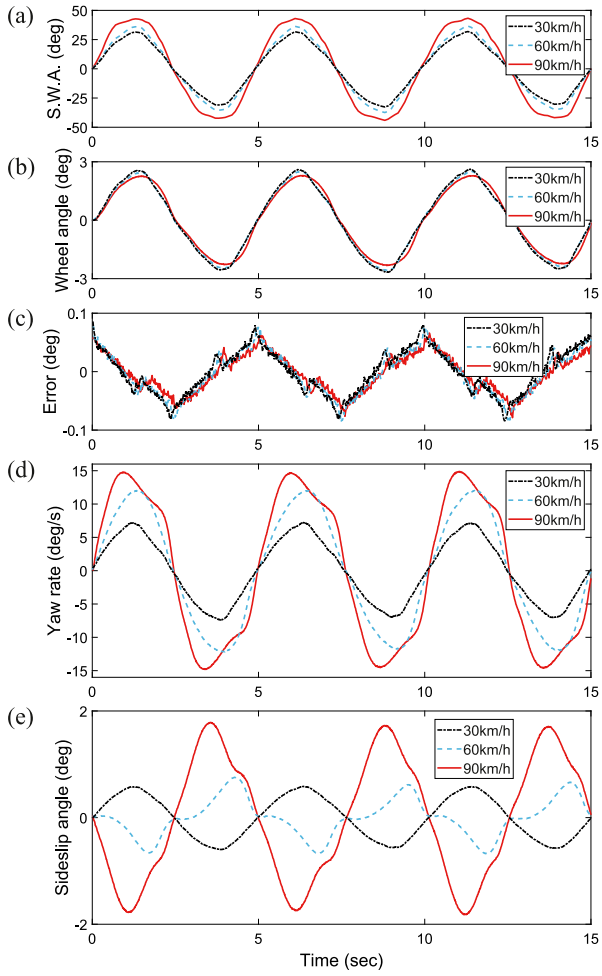

Fig. 16. Comparison of weave test results with different vehicle forward speeds. (a) Steering wheel angle. (b) Front wheel angle. (c) Tracking error. (d) Yaw rate. (e) Sideslip angle.

Fig. 14, the SbW experimental platform used in this research comprises a software part and a hardware part. In the software part, a real-time control prototype (dSPACE DS2211) is adopted as the central controller, and the algorithm model is established in Matlab/Simulink. Besides, Carsim is used to implement the full vehicle dynamics model and transfer vehicle states to the algorithms in dSPACE. The hardware part contains the steering wheel module and the steering actuator module. Driver's inputs are collected by the wheel angle sensor and transmitted to the Micro-Autobox in the steering wheel module. In the steering actuator module, the SbW system ECU receives the signals of reference front wheel angle & control torque and transmits the information to the steering motor. Also, the actual front angle is calculated by signals of the rack stroke sensor and then fed back to the dSPACE. The parameters specification of vehicle model and steering actuating system is the same as Table 2. The system sampling time is chosen as 10 ms with the CAN bus communication applied in experiments.

According to ISO standards for the vehicle, several driving conditions are presented as examples for the HiL experiments: two open loop test cycles, i.e., Weave Test [30] and Transition Test [31] are basic steering tests with the relative small steering wheel angle; Square Turn Test and Serpentine Test [32] are two critical steering tests, with the high steering velocity and large disturbances. To demonstrate the improvement of the designed handling stability control strategy, the sliding-mode-based wheel angle compensation method [15] with the fixed transmission ratio and a SMC-KL tracking controller are employed as the contrastive control scheme. Considering the VSR strategy and the time-varying wheel angle compensation would lead to different steering inputs, we selected the steering command from the steering wheel input to the actuator as the standard steering angle in test cycles. The main characteristic values of test cycles mentioned above are given in Table 5.

Fig. 15 shows the HiL experimental results of the weave test. As shown in Fig. 15(a), the steering wheel angle under two schemes are almost the same, indicating that the VSR strategy presents a balance between steering sensitivity and driving stability with small angle at 60 km/h. Fig. 15(b) presents the front wheel angle. Fig. 15(c) shows that the proposed ATC has better tracking performance. As shown in Fig. 15(d), the vehicle yaw rate under the proposed control scheme (c.s.) shows a rather smooth change, whereas, the yaw rate under the contrastive c.s. appears relatively irregular fluctuations in every period. Besides, the sideslip angle based on the proposed c.s. is much smaller with steadier variations in Fig. 15(e). Fig. 15(d) and (e) reflect that the vehicle shows better steering stability performance with the proposed c.s..

Fig. 16 presents the comparison of weave test results by different vehicle forward speeds based on the proposed c.s.. As shown in Fig. 16(a), the VSR strategy tends to improve the handling stability at high speeds, so that the transmission ratio increases with the rising of vehicle speed. Fig. 16(b) shows the actual front wheel angle. Fig. 16(c) illustrates that the proposed ATC maintains good tracking performance at various vehicle forward speeds. Both the vehicle yaw rate and the sideslip

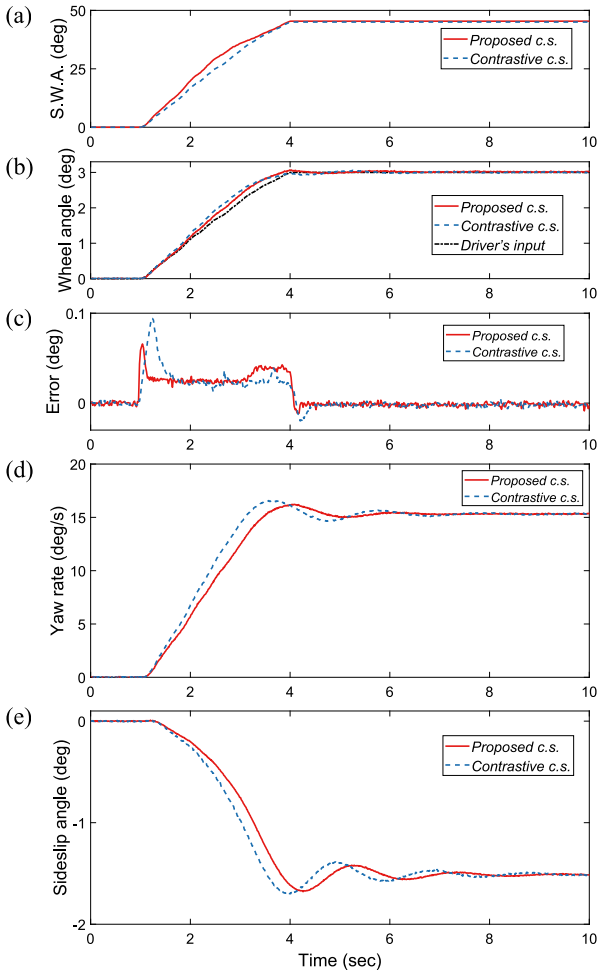

Fig. 17. 15°/s transition test at vehicle forward speed 80 km/h. (a) Steering wheel angle. (b) Front wheel angle. (c) Tracking error. (d) Yaw rate. (e) Sideslip angle.

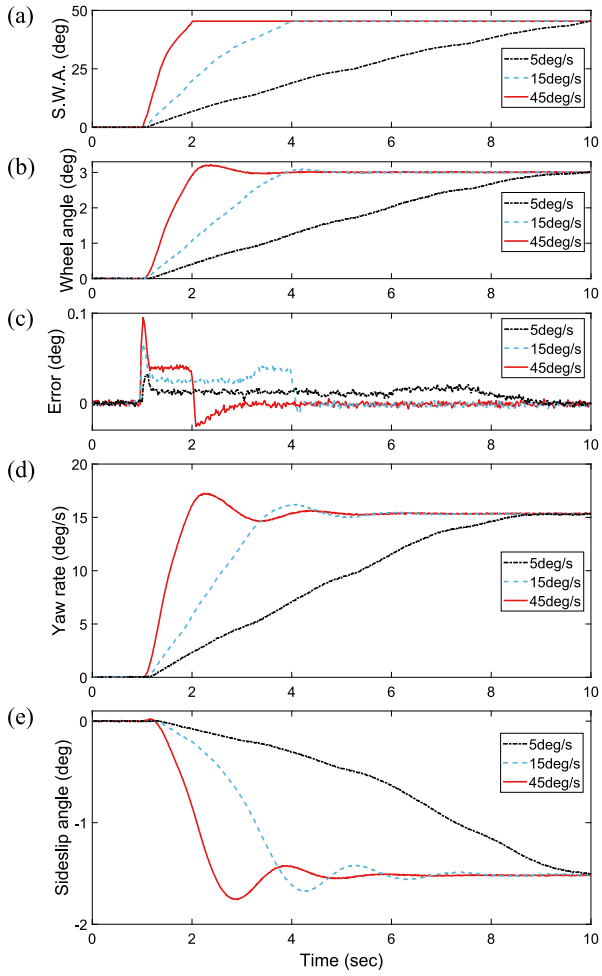

Fig. 18. Comparison of transition test results with different steering angular velocities. (a) Steering wheel angle. (b) Front wheel angle. (c) Tracking error. (d) Yaw rate. (e) Sideslip angle.

angle change smoothly, as shown in Fig. 16(d) and (e), indicating the proposed c.s. effectively enhances the driving stability at different vehicle speeds. It is interesting to be observed that responses of vehicle yaw rate and sideslip angle in Fig. 16(d) and (e) present a same trend at low speeds, whereas an opposite one at high speeds due to the change of stable point positions in the "sideslip angle – yaw rate" phase diagram.

Fig. 17 presents the HiL experimental results of the transition test. The steering wheel angle and the front wheel angle are shown in Fig. 17(a) and (b), respectively. Fig. 17(c) shows the better tracking performance of SbW system under the proposed c.s.. It can be found that the response of yaw rate under the proposed c.s. in Fig. 17(d) converges to the desired value faster with relatively smaller oscillations. Similarly, the vehicle sideslip angle based on the proposed c.s. converges at around t=7s, whereas the sideslip angle under the contrastive c.s. oscillates until the end of the test. Fig. 17(d) and (e) illustrate the proposed c.s. can help vehicles reach the stable states faster during the emergency steering.

Fig. 18 shows a comparison of HiL transition test results by different steering angular velocities under the proposed c.s.. Fig. 18(a) and (b) present the steering wheel angle and the actual front wheel angle, respectively. The instantaneous error at t=1s increases with the growth of the steering angular velocity, as shown in Fig. 18(c), but the tracking performance is satisfactory on the whole. Although the response of the vehicle yaw rate in Fig. 18(d) oscillates violently at the high steering angular velocity, which also converge to the desired value in limited time. The sideslip angle response in Fig. 18(e) present the similar convergence characteristics with an opposite tendency. On the whole, Fig. 18(d) and (e) demonstrate that the proposed c.s effectively improve the vehicle steering stability performance.

Fig. 19 presents the HiL experimental results of the square turn test. As shown in Fig. 19(a), the relative small steering wheel angle is required in the proposed c.s., demonstrating that the VSR strategy enhances the steering agility. It can be observed that the front wheel angle of both schemes are less than the driver's input in Fig. 19(b), which reveals that the AFS controller prefer to reduce the steering angle in critical driving conditions. Fig. 19(c) shows that the proposed ATC maintains excellent tracking performance even with the quite high steering velocity. As shown in Fig. 19(d), the vehicle yaw rate displays a smooth change based on the proposed c.s.. In contrast, the yaw rate under the contrastive c.s. shows excessive fluctuations, especially when the rotation direction of the steering wheel turns abruptly. Besides, the sideslip angle under the proposed c.s. presents a significantly steadier change compared with the one under the contrastive c.s. in Fig. 19(e), indicating a great improvement in vehicle stability performance of the proposed c.s..

Fig. 20 shows the HiL experimental results of the serpentine test. The steering wheel angle and the front wheel angle in the test are listed in Fig. 20(a) and (b), respectively. The proposed ATC presents great tracking performance even with large disturbances, as shown in Fig. 20(c). In Fig. 20(d), the vehicle yaw rate oscillates under

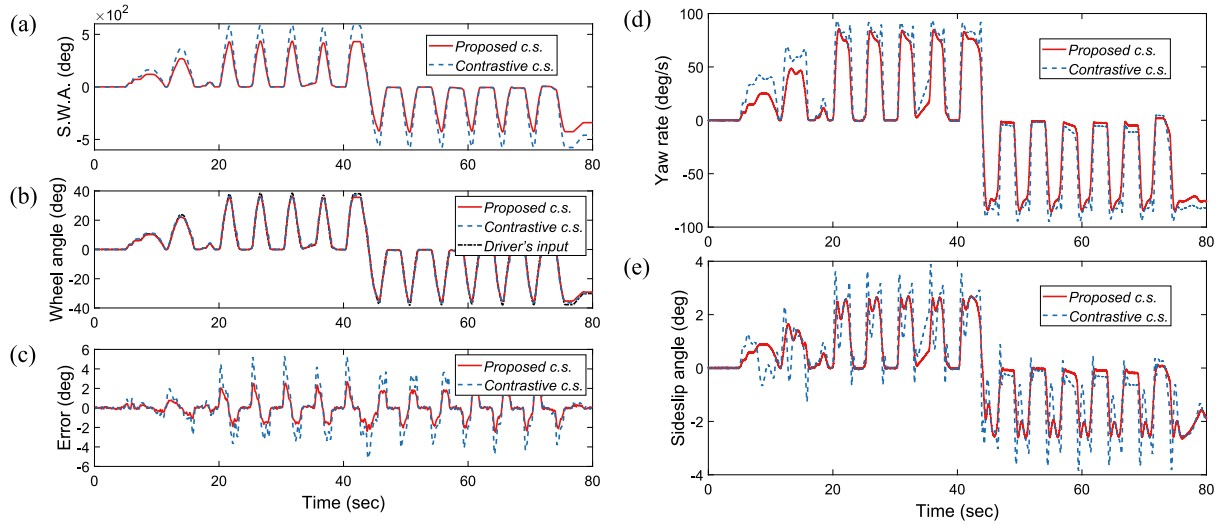

Fig. 19. Square turn test at vehicle forward speed 60 km/h with the road adhesion set as 0.8. (a) Steering wheel angle. (b) Front wheel angle. (c) Tracking error. (d) Yaw rate. (e) Sideslip angle.

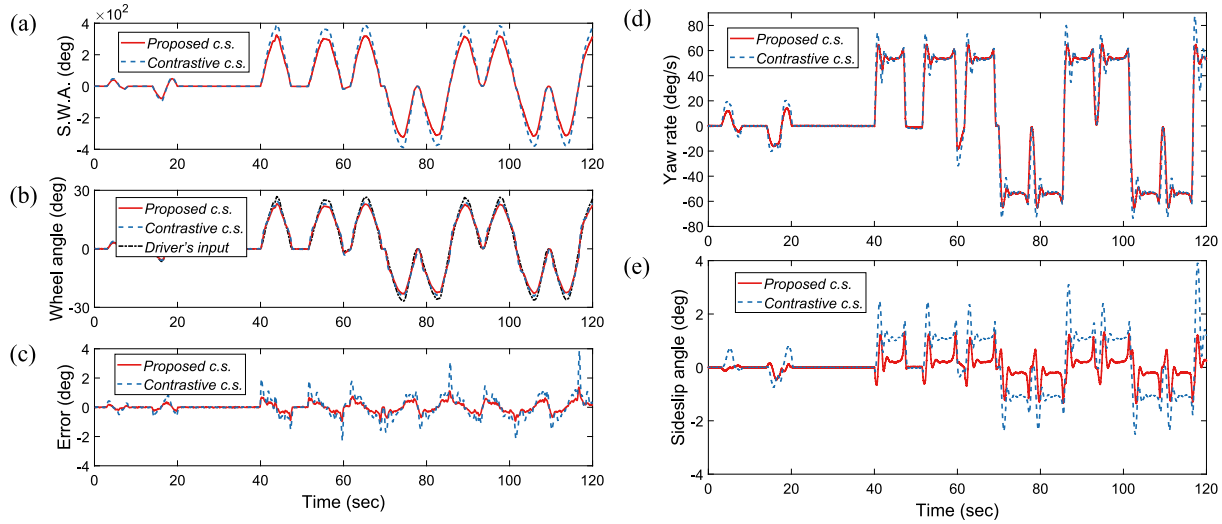

Fig. 20. Serpentine test at vehicle forward speed 40 km/h with the road adhesion set as 0.4. (a) Steering wheel angle. (b) Front wheel angle. (c) Tracking error. (d) Yaw rate. (e) Sideslip angle.

both control schemes when the steering wheel rotation direction turns swiftly, however, the yaw rate under the proposed c.s. can converge to the stable value more quickly. Similarly, the sideslip angle under the proposed c.s. converges faster, as shown in Fig. 20(e). Also, the sideslip angle based on the proposed c.s. remains between ± 2deg with significantly steadier fluctuations. Based on the above analyses, the proposed c.s. effectively improve the vehicle driving stability performance, even in the extreme driving conditions.

5. Conclusions

In this paper, a novel adaptive hierarchical control approach of the handling stability improvement in SbW vehicles is proposed. The high-level control scheme comprised of the VSR strategy and an AFS controller is designed to improve the steering stability with the generated desired front wheel angle, meanwhile the ATC is introduced to ensure the accuracy tracking performance of the SbW system in the low-level. In comparison with other existing sliding-mode based control methods, such as the SMC-KL steering controller, simulation and experimental results demonstrate that the designed control scheme can achieve the excellent handling stability and tracking performance in different driving scenarios, even in some critical steering conditions. In the further study, the steering modeling with tyre dynamics will be considered in the control structure to improve the handling stability of SbW vehicles, and more vehicle experiments and evaluation will be conducted to further validate the proposed control strategy.

CRediT authorship contribution statement

Haohan Yang: Conceptualization, Methodology, Software, Writing - original draft. **Wentong Liu:** Conceptualization, Data curation, Investigation, Validation. **Li Chen:** Supervision, Funding acquisition. **Fan Yu:** Supervision, Writing- review & editing.

Declaration of competing interest

The authors declare that they have no known competing financial interests or personal relationships that could have appeared to influence the work reported in this paper.

Acknowledgment

This work is supported by National Nature Science Foundation of China (Grant No. 51875340).

References

[1] Inagaki T. Smart collaboration between humans and machines based on mutual understanding. Annu Rev Control 2008;32(2):253–61.
[2] Shimizu Y, Kawai T, Yuzuriha J. Improvement in driver-vehicle system performance by varying steering gain with vehicle speed and steering angle: VGS (variable gear-ratio steering system) 1999. No. 1999-01-0395. SAE Technical paper.
[3] Kim S, Kwak B, Chung S, et al. Development of an active front steering system. Int J Automot Technol 2006;7(3):305–10.
[4] Ma X, Wong PK, Zhao J, et al. Multi-objective sliding mode control on vehicle cornering stability with variable gear ratio actuator-based active front steering systems. Sensors 2016;17(1):49–64.
[5] Azzalini M, Gissinger GL, Boussouar V, et al. Computation of a variable steering ratio with a fuzzy logic method. In: 13th Intelligent vehicle symposium. New York: IEEE; 2002, p. 259–67.
[6] Wu X, Li W. Variable steering ratio control of steer-by-wire vehicle to improve handling performance. Proc Inst Mech Eng D 2020;234(2):774–82.
[7] Falcone P, Borrelli F, Asgari J, et al. Predictive active steering control for autonomous vehicle systems. IEEE Trans Control Syst Technol 2007;15(3):566–80.
[8] Nam K, Oh S, Hori Y. Robust yaw stability control for electric vehicles based on active steering control. Int J Automot Technol 2012;13(7):1169–76.
[9] Doumiati M, Sename O, Dugard L, et al. Integrated vehicle dynamics control via coordination of active front steering and rear braking. Eur J Control 2013;19(2):121–43.
[10] Zhang H, Wang J. Vehicle lateral dynamics control through AFS/DYC and robust gain-scheduling approach. IEEE Trans Veh Technol 2016;65(1):489–94.
[11] Her H, Koh Y, Joa E, et al. An integrated control of differential braking, front/rear traction, and active roll moment for limit handling performance. IEEE Trans Veh Technol 2016;65(6):4288–300.
[12] Zhao J, Wong P, Ma X, et al. Chassis integrated control for active suspension, active front steering and direct yaw moment systems using hierarchical strategy. Veh Syst Dyn 2017;55(1):72–103.
[13] Yoshimura T. Discrete-time adaptive sliding mode controller for vehicle steering systems with preview. J Vib Control 2012;19(10):1587–600.
[14] Diao X, Jin Y, Ma L, et al. Composite active front steering controller design for vehicle system. IEEE Access 2017;5(1):6697–706.
[15] Etienne L, Acosta C, Gennaro S, et al. A super-twisting controller for active control of ground vehicles with lateral tire-road friction estimation and carsim validation. Int J Control Autom 2020;18(5):1177–89.
[16] Wang X, Zong C, Xing H, et al. Bilateral control method of torque drive/angle feedback used for steer-by-wire system. SAE Int J Passeng Cars Electron Electr Syst 2012;5(2):479–85.
[17] Cetin A, Adli M, Barkana D, et al. Implementation and development of an adaptive steering-control system. IEEE Trans Veh Technol 2010;59(1):75–83.
[18] Cetin A, Adli M, Barkana D, et al. Adaptive on-line parameter identification of a steer-by-wire system. Mechatronics 2012;22(2):152–66.
[19] Wang H, Man Z, Shen W, et al. Robust control for steer-by-wire systems with partially known dynamics. IEEE Trans Ind Electron 2014;10(4):2003–15.
[20] Wang H, Man Z, Kong H, et al. Design and implementation of adaptive terminal sliding-mode control on a steer-by-wire equipped road vehicle. IEEE Trans Ind Electron 2016;63(9):5774–85.
[21] Zhu G, Yang H, Yu F. Controller design for an automobile steer-by-wire system. In: 28th International symposium on industrial electronics. New York: IEEE; 2019, p. 1492–7.
[22] Lin F, Hung Y, Ruan K. An intelligent second-order sliding-mode control for an electric power steering system using a wavelet fuzzy neural network. IEEE Trans Fuzzy Syst 2014;22(6):1598–611.
[23] Wang H, Xu Z, Do MT, et al. Neural-network-based robust control for steer-by-wire systems with uncertain dynamics. Neural Comput Appl 2015;26(7):1575–86.
[24] Zhang J, Wang H, Ma M, et al. Active front steering-based electronic stability control for steer-by-wire vehicles via terminal sliding mode and extreme learning machine. IEEE Trans Veh Technol 2020;53(4):939–46.
[25] Yu F. Vehicle system dynamics and control. 2nd ed. Beijing: China Machine Press; 2010.
[26] Road vehicles lateral transient response test methods open-loop test methods. 2011, ISO 7401.
[27] Jang J. ANFIS: adaptive-network-based fuzzy inference system. IEEE Trans Syst Man Cybern 1993;23(3):665–85.
[28] Edwards C, Spurgeon S. Sliding-mode control: theory and applications. 1st ed. New York: Taylor & Francis; 1988.
[29] Passenger cars test track for a severe lane-change maneuver part 2: Obstacle avoidance. 2002, ISO 3888-2.
[30] Road vehicles test method for the quantification of on-centre handling part 1: Weave test. 2003, ISO 13674-1.
[31] Road vehicles test method for the quantification of on-centre handling part 2: Transition test. 2006, ISO 13674-2.
[32] Controllability and stability test procedure for automobile. 2014, GB/T 6323-2014.

Haohan Yang received the B.S. degree in mechanical engineering from the Dalian University of Technology, Dalian, China, in 2018. He is currently working toward the master's degree in vehicle engineering with Shanghai Jiao Tong University, Shanghai, China. His current research interests include vehicle system dynamics and intelligent vehicle control.

Wentong Liu received the B.S. and M.S. degree in marine engineering from the Shanghai Jiao Tong University, Shanghai, China, in 2018 and 2021, respectively. He is currently a senior engineer at National Engineering Laboratory for Marine and Ocean Engineering Power System. His current research interests include steer-by-wire system development of automobile vehicles and motion control.

Li Chen received the B.S. and M.E. degrees in mechanical engineering from the Hunan University, Changsha, China, in 1994 and 1997, respectively, and the Ph.D. degree in vehicle engineering from the Shanghai Jiao Tong University, Shanghai, China, in 2000.

She is currently an Associate Professor with the School of Naval Architecture, Ocean & Civil Engineering, Shanghai Jiao Tong University, Shanghai, China. She has contributed to more than 70 publications and 9 invention patents. Her research interests include adaptive control, advanced powertrain systems, and mechatronics.

Fan Yu received the B.S. and M.E. degrees in mechanical engineering from the Jilin University of Technology, Changchun, China, in 1982 and 1987, respectively, and the Ph.D. degree in vehicle engineering from the University of Leeds, Leeds, U.K., in 1996.

She is currently a Professor with the Institute of Intelligent Vehicle, Shanghai Jiao Tong University, Shanghai, China. She has contributed to more than 180 publications and holds 9 granted China patents. Her current research interests include vehicle dynamics and control, vehicle chassis control system, and intelligent vehicle control.